IEEE Access
Multidisciplinary ⋮ Rapid Review ⋮ Open Access Journal

Received 17 September 2023, accepted 4 November 2023, date of publication 8 November 2023,
date of current version 14 November 2023.

Digital Object Identifier 10.1109/ACCESS.2023.3331152

RESEARCH ARTICLE

Crack Defect Detection Processing Algorithm and Method of MEMS Devices Based on Image Processing Technology

YU ZHENG, SUSU LI, YUAN XIANG, AND ZHENXING ZHU

Science and Technology on Reliability Physics and Application Technology of Electronic Component Laboratory, East China Institute of Photo-Electron IC, Bengbu 233000, China

Corresponding author: Yu Zheng (zhengyu0905@yeah.net)

This work was supported by the Project of Science and Technology on Reliability Physics and Application Technology of Electronic Component Laboratory under Grant 2022-JCJQ-LB-067/6142806220301.

ABSTRACT In order to solve the problem that the crack defects generated on the surface of MEMS devices are difficult to detect under high overload impact, this paper proposes a crack detection method based on attribute weighted naive Bayes improved OTSU algorithm. Based on the analysis of the surface defects in MEMS devices image, the edge information of the crack defect in the image is extracted by image processing such as image detail sharpening, grayscale processing, image enhancement and edge extraction based on Canny operator, and the pseudo crack in the image is removed by the least square method; the attribute weighted naive Bayes algorithm is introduced to improve the traditional OTSU image processing method, the crack defect detection results of the MEMS devices image are obtained, the crack defects are quantitatively characterized, and the length and width of the crack defects are calculated. Comparative experiments were conducted using multiple detection methods, the results showed that the crack detection method proposed in this paper can obtain the crack defect information of MEMS devices efficiently and accurately.

INDEX TERMS MEMS devices, crack defect detection, image segmentation, quantitative characterization.

I. INTRODUCTION

The modules of Micro-Electro-Mechanical-Systems (MEMS) mainly include micro-sensor, signal processing circuits and micro-actuators, etc. [1], [2], [3], and the size of these modules is between a few microns and a few millimeters, with the characteristics of miniaturization, high precision, high reliability and low power consumption [4], [5]. Nowadays MEMS devices are widely used in aerospace, medical, military and other fields, and have important application value [6], [7], [8]. MEMS devices play a crucial role in various application scenarios; they must deal with a variety of complex environments, so that their entire life cycle will be subjected to temperature, humidity, vibration, shock, radiation and other environmental stresses independent or coupled effects. In the field of weapon testing, due to the phenomenon of high overload during the launch of the projectile, under the action of high overload, it is easy to cause the phenomenon of high temperature burning or extrusion of MEMS devices in the missile-borne actuator, which makes the chip pin fall off or the surface crack and other defects, which will cause the missile-borne actuator to lose its own performance. Therefore, in the missile-borne test experiment, a high overload experiment is often required. The performance change of the MEMS device is observed by applying a high acceleration simulation experiment to the MEMS device. After the simulation experiment, the MEMS device after high acceleration impact is removed, and the defects on the chip surface are detected by artificial or machine vision methods.

In traditional experiments, manual detection is used to detect defects. However, manual detection has many variable factors and cannot quantitatively describe defects, which affects the accuracy and reliability of detection. Therefore, manual detection has a significant subjective impact, poor real-time performance, high labor intensity and high false detection rate. With the development of computer image

The associate editor coordinating the review of this manuscript and approving it for publication was Sudhakar Radhakrishnan.

processing technology, the method of using machine vision equipment such as metallographic microscopy, ultrasonic scanning and X-ray scanning to obtain images and judge the surface defect information in the images has been developed [9]. The introduction of machine vision reduces the manual operation of surface defect detection and improves the automation level of the detection process. In recent years, many scholars have conducted relevant research on defect detection based on machine vision. Yuan et al. [10] proposed a tire appearance defect detection method combining Histogram of Oriented Gradient (HOG) and Local Binary Pattern (LBP) features. Firstly, a tire image data set is constructed to provide defective and normal tire images. Then, the HOG and LBP features of the tire image are extracted respectively to train the Support Vector Machine (SVM) classifier. Finally, the SVM classifier combines HOG and LBP feature to calculate the prediction scores of the test image. These scores can be used to determine whether the test image is a defective tire image or a normal tire image, so as to achieve the purpose of tire appearance defect detection. Aiming at the problem of surface defects of stamping blanks, Shang et al. [11] proposed a method for detecting surface defects of stamping blanks by combining Normalization Cross Correlation (NCC) template matching accelerated based on Gaussian pyramid and background subtraction. In order to segment defects from complex rail surface images during high-speed motion, He et al. [12] established a background model of rail surface images based on the fact that the rail surface images have basically unchanged pixel values along the rail direction, and proposed a rail surface defect detection algorithm based on background difference. To a certain extent, this method solves the influence of adverse factors such as image illumination changes, uneven reflection, and few features during the segmentation of rail surface defects. Guo et al. [13] proposed a method for surface defect detection of ceramic bowls based on machine vision. This method mainly realizes the edge detection of surface defects by combining Kirsch operator and Canny operator. It is difficult for traditional image processing algorithms to effectively deal with the problems of uneven illumination or serious noise interference in subway tunnel crack defect images. Liu et al. [14] studied an improved crack detection algorithm based on structural analysis based on pixel-level processing to improve the quality of tunnel images. In terms of using image processing methods to detect electronic components, Jung et al. [15] used the camera system to capture the defect data image of the plate product. By analyzing and processing the images, they proposed crack detection technology based on image processing. The detection method mainly locates the defect position of the electronic components and realizes the crack defect detection. Lv et al. [16] proposed to use Canny-region splitting and merging algorithm to detect surface defects such as scratches and dirt on the surface of electronic components. Although there are many good ideas and methods to detect defects by using image processing technology, there is no relevant reference on the detection of crack defects of the surface of MEMS devices under high overload. Moreover, due to the fact that the surface of the MEMS devices is actually a metal surface, there is a reflection effect and the defect characteristics are not obvious, it is difficult to locate during detection, which is easy to cause false detection and missed detection, and the detection is difficult. According to the analysis of surface defects of MEMS devices, this paper proposes a crack detection method based on attribute weighted naive Bayes improved OTSU algorithm, and quantitatively characterizes the crack on the basis of extracting the crack skeleton. These information can provide data basis for detecting the failure of MEMS devices under high overload.

The main contributions and highlights of this paper are:

(1) According to the analysis of MEMS devices image surface defects, the defect edge information in the image is extracted by image detail sharpening, grayscale processing, image enhancement and edge extraction based on Canny operator, and the pseudo crack in the image is removed by least square method.

(2) Based on the traditional OTSU image processing method, the attribute weighted naive Bayes algorithm is introduced to improve the OTSU algorithm, and the crack defect detection results of MEMS devices images are obtained.

(3) The Zhang-Suen thinning algorithm is used to extract the crack skeleton of the MEMS devices image, and the calculation model of the length and width of the crack is established.

The structure of the paper is arranged as follows: Section II introduces the detailed process of image processing of MEMS devices. Section III gives the crack defect detection method of MEMS devices image. Section IV describes the quantitative characterization calculation method of crack defects of MEMS devices image. Section V gives the experiment and result analysis of crack defects of MEMS devices image. Section VI gives a summary.

II. THE SURFACE DEFECT ANALYSIS AND IMAGE PROCESSING OF MEMS DEVICES

A. ANALYSIS OF SURFACE DEFECTS OF MEMS DEVICES

MEMS devices usually work in a resonant state. During the working process, the movable parts carry out cyclic mechanical movements in specific forms, such as stretching, compression, bending, vibration, thermal expansion and thermal contraction [17], the alternating stress will gradually accumulate the fatigue damage of the material, resulting in cracks, and even lead to structural fracture, make the MEMS device unusable. Figure 1 (a) shows that a curved crack is generated inside the MEMS device under high overload. Cracks will propagate from the surface of the MEMS device along the thickness direction, which makes the MEMS device have serious reliability problems and affects its normal operation. Figure 1 (b) shows that there are cracks between the two metals in the MEMS device. The cracks will form an electrical path between the two strips of metal, resulting in a short circuit during normal operation of the MEMS device.

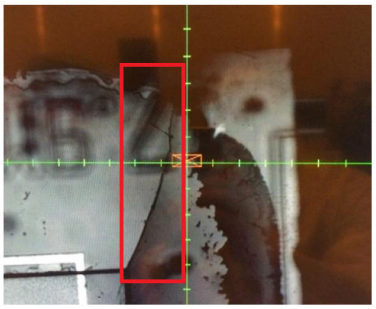

(a) A curved crack image on the surface of the MEMS device

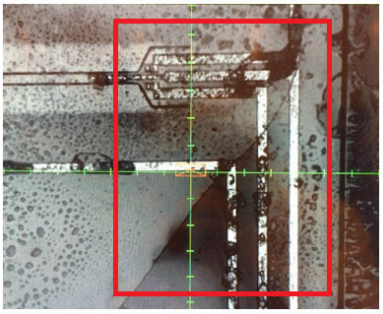

(b) There is a crack image between the two metals on the surface of the MEMS device

FIGURE 1. Surface crack defect image of MEMS device.

The crack defects caused by stress sensitivity are often related to the production environment, processing technology and micro-component materials of the MEMS device, and even involve the design of molds or micro-component structures. In Figure 1, there are some crack defects in the red frame.

B. MEMS DEVICES IMAGE PROCESSING

In order to eliminate the defect-independent information in the MEMS devices image and improve the detection accuracy of the surface defects in the MEMS devices image, the image needs to be processed. The specific process is shown in Figure 2.

1) IMAGE DETAIL SHARPENING

The MEMS devices images are inevitably blurred during the collection process. In order to enhance the detail information of the MEMS devices image and highlight the edge details of the surface crack of MEMS devices, bilateral filtering is used to sharpen the MEMS devices images. The spatial proximity of the collected image and the pixel value are taken as the weight conditions, which not only considers the Euclidean distance of the pixel space domain, but also considers the difference of the gray value in the pixel range domain [18], so as to realize the filtering and denoising processing under the condition of ensuring the edge information of the image.

Suppose that (i_0, j_0) is the coordinates of the central pixel, (a, b) is the coordinates of one pixel in the neighborhood of (i_0, j_0) and $g_p(i_0, j_0)$ is the gray prediction value of the central pixel, then

$$g_p(a,b) = \frac{\sum_{a,b} F(a,b)W(i_0,j_0,a,b)}{\sum_{a,b} W(i_0,j_0,a,b)} \tag{1}$$

where $F(a, b)$ is the gray value of the neighborhood pixel; the weighting coefficient $W(i_0, j_0, a, b)$ is the comprehensive result of the spatial domain kernel and the pixel range domain kernel. The expressions of the spatial domain kernel and the pixel range domain kernel are shown in formulas (2) and (3).

$$S(i_0,j_0,a,b) = \exp\left[-\frac{(i_0-a)^2+(j_0-b)^2}{2\sigma_r^2}\right] \tag{2}$$

$$I(i_0,j_0,a,b) = \exp\left[-\frac{\|F(i_0,j_0)-F(a,b)\|^2}{2\sigma_s^2}\right] \tag{3}$$

where σ_r and σ_s are spatial standard deviation and gray standard deviation, respectively.

Bilateral filtering is a compromise processing method by combining the spatial proximity of the image and the similarity of the pixel values, and taking into account the spatial information and gray similarity to achieve the purpose of edge preservation and denoising. Figure 3 (a) is the detail sharpening processing result of MEMS devices image (curved cracks), and Figure 3 (b) is the detail sharpening processing result of MEMS devices image (cracks penetrating between two metals).

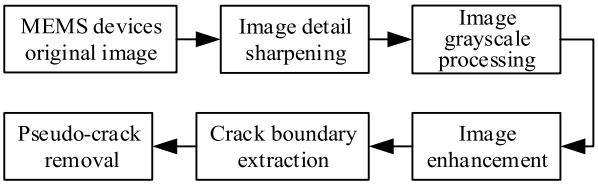

FIGURE 2. Image processing flow chart.

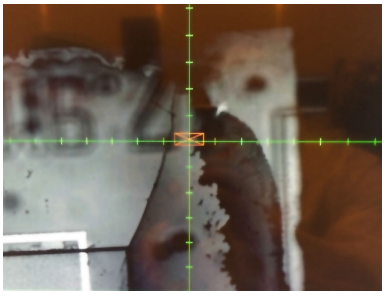

(a) The detail sharpening processing result of MEMS devices image (curved cracks)

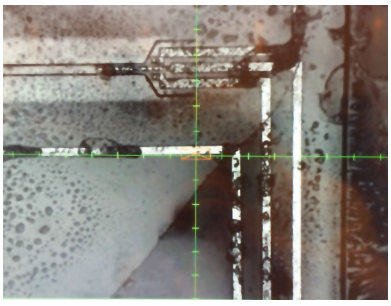

(b) The detail sharpening processing result of MEMS devices image (cracks penetrating between two metals)

FIGURE 3. MEMS devices image detail sharpening effect.

It can be seen from Figure 3 that bilateral filtering can not only sharpen the surface crack details of MEMS devices image and highlight the surface crack characteristics of components, but also reduce the influence of surface stains and other factors on the image.

2) IMAGE GRAY PROCESSING

The original images of MEMS devices collected in this paper are all color images. The color images are synthesized by red, green and blue colors, which are also called RGB images. Because the color features of the crack of MEMS devices image are not rich, the MEMS devices image is grayed, that is, the RGB color image is converted into a grayscale image, which not only retains the main features of the image, but also reduces the computational cost of the computer.

If any pixel in the image is defined as (i, j), and the gray value here is $Gray(i, j)$, the values corresponding to the three color channels are $R(i, j)$, $G(i, j)$, $B(i, j)$, respectively. The corresponding weights are $\kappa_1, \kappa_2, \kappa_3$, respectively. These weights satisfy $\kappa_1 + \kappa_2 + \kappa_3 = 1$. The appropriate weighted average of RGB three primary color components can obtain the best gray image.

$$Gray(i, j) = \kappa_1 \cdot R(i, j) + \kappa_2 \cdot G(i, j) + \kappa_3 \cdot B(i, j) \tag{4}$$

The MEMS device image after sharpening process is implemented by the weighted average grayscale method [19], and the converted grayscale image is shown in Figure 4.

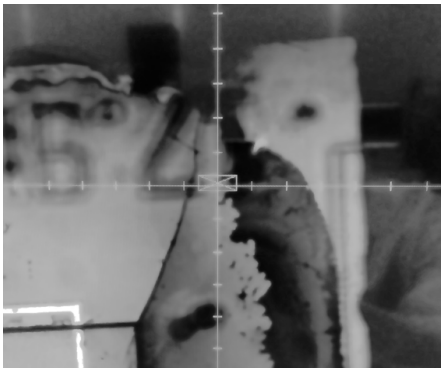

(a) Grayscale processing result of MEMS devices Image (curved cracks)

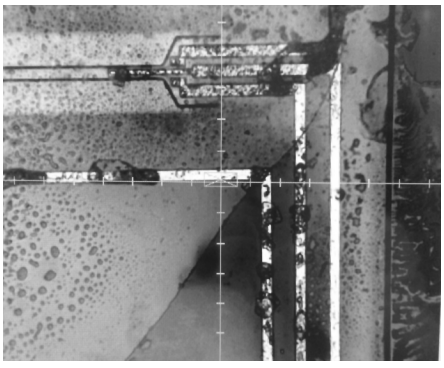

(b) Grayscale processing result of MEMS devices Image (cracks penetrating between two metals)

FIGURE 4. Grayscale processing of MEMS devices Image.

3) IMAGE ENHANCEMENT

In order to improve the unobvious defect features in MEMS devices image, it is necessary to improve the contrast of MEMS devices images. Taking any point $x(i, j)$ of the image as the center, in the area with a window size of $(2n + 1) \times (2n + 1)$, the local mean and variance can be expressed as:

$$h_x(i, j) = \frac{1}{(2n+1)^2} \sum_{k=i-n}^{i+n} \sum_{l=j-n}^{j+n} x(k, l) \tag{5}$$

$$\sigma_x^2(i, j) = \frac{1}{(2n+1)^2} \sum_{k=i-n}^{i+n} \sum_{l=j-n}^{j+n} [x(k, l) - h_x(i, j)]^2 \tag{6}$$

where $h_x(i, j)$ is the mean value, which can be approximately considered as the background part; $x(k, l)$ is the pixel value in the $(2n + 1) \times (2n + 1)$ region; $\sigma_x^2(i, j)$ is the local variance [20]. At this time, $x(k, l) - h_x(i, j)$ is the high-frequency detail part, and the gain product of the high frequency is:

$$f(i, j) = h_x(i, j) + G(i, j)[x(i, j) - h_x(i, j)] \tag{7}$$

where $f(i, j)$ is the value after gain.

Based on Figures 4 (a) and 4(b), the effect of image enhancement is shown in Figure 5.

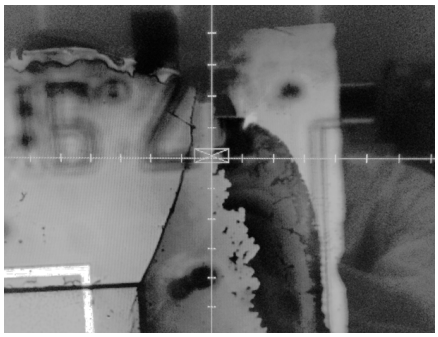

(a) Image enhancement processing result of MEMS devices (curved cracks)

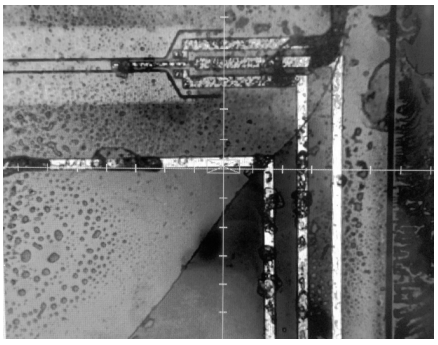

(b) Image enhancement processing result of MEMS devices (cracks penetrating between two metals)

FIGURE 5. Image enhancement processing result of MEMS devices.

Comparing figures 3,4 and 5, it can be seen that after the image enhancement processing of the collected MEMS devices images, the crack defect contour is clearer, which effectively improves the contrast of the image and provides

more useful information for the boundary extraction of the next crack defect.

4) CRACK DEFECT BOUNDARY EXTRACTION

In order to realize the extraction of the image area of the MEMS devices, the detected crack edge pixels and their surrounding pixels are defined as sensitive areas and positioned by detecting the crack edge or linear characteristics. Based on Canny operator detection algorithm, the crack edge of MEMS devices image is roughly extracted. The specific steps are as follows:

(1) In order to remove noise, Gaussian filtering is used to smooth the MEMS devices images [21].

Firstly, the original color image of the MEMS devices is grayed, and then the MEMS devices image is denoised by convolution operation with Gaussian function.

$$h(x, y) = \exp\left(-\frac{x^2 + y^2}{2\sigma^2}\right) \tag{8}$$

$$g(x, y) = h(x, y) * f(x, y) \tag{9}$$

where $h(x, y)$ is the Gaussian function of the omitted coefficient; $f(x, y)$ is the grayscale image and $g(x, y)$ is the smoothed image.

(2) Calculate the amplitude and direction of the gradient.

The direction of calculating the gradient is to find the position where the gray value changes the most in the image. The calculated amplitude of the gradient is:

$$\varphi(x, y) = \sqrt{\varphi_1^2(x, y) + \varphi_2^2(x, y)} \tag{10}$$

The direction of the gradient is:

$$\theta_\varphi = \tan^{-1} \frac{\varphi_2(x, y)}{\varphi_1(x, y)} \tag{11}$$

where $\varphi_1(x, y) = f(x, y) * h_1(x, y), \varphi_2(x, y) = f(x, y) * h_2(x, y), h_1 = \begin{vmatrix} -1 & -1 \\ 1 & 1 \end{vmatrix}, h_2 = \begin{vmatrix} 1 & -1 \\ 1 & -1 \end{vmatrix}$.

(3) Non-maximum suppression of amplitude.

After the gradient is calculated, the crack edge cannot be determined immediately. The point with the largest local gradient needs to be retained and the local non-maximum value needs to be set to zero.

(4) Double threshold detection edge.

The two thresholds of T_1 and T_2 are used to detect the edge, where $T_1 < T_2$, the edge pixel with a gradient greater than T_2 is a strong edge point. If it is between T_2 and T_1, this point is a weak edge point. If the gradient value of the pixel is less than T_1, it is considered that this point is not an edge point and suppresses this point. For weak edge points, it is not sure whether they are edge points, so it is necessary to judge by searching the eight connected regions of pixels, which can get two threshold edge images.

Based on Figure 5, the results of Canny operator to extract its edge features are shown in Figure 6.

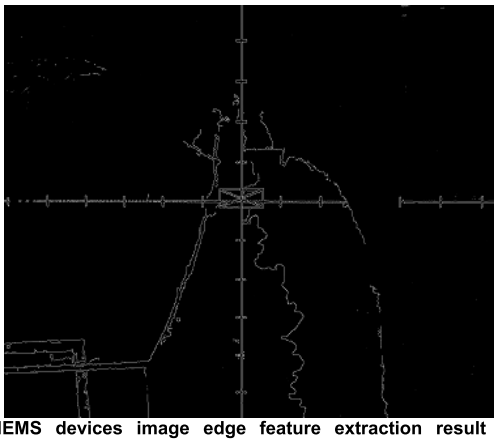

(a) MEMS devices image edge feature extraction result (curved cracks)

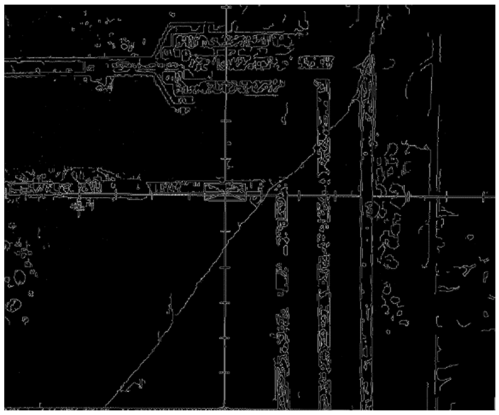

(b) MEMS devices image edge feature extraction results (cracks penetrating between two metals)

FIGURE 6. The edge feature extraction results of MEMS devices image.

5) PSEUDO CRACK DEFECT REMOVAL

There is false crack information in the images of MEMS devices taken by imaging equipment, which are horizontally or vertically distributed with the longitudinal axis of the device, and are similar to the gray scale of crack defects. In order to prevent false cracks from being misjudged as cracks in crack detection and improve the segmentation accuracy of image segmentation, false cracks are removed by image processing methods. From the morphological properties of the crack and the pseudo-crack formed by the tangent, the variance of the pixel distribution of the crack and the pseudo-crack can be calculated by the least square method. The variance of the pixel distribution of the pseudo-crack formed by the tangent is linearly related to the tangent length, and the distribution variance of the pseudo-crack is very small. On the contrary, the real crack is random and uncertain, and the variance of the distribution of different crack pixels is not related to the length, and the variance of the crack distribution is large. The steps of the pseudo crack removal algorithm are as follows:

(1) Based on the MEMS devices image extracted from the edge of the crack defect, the MEMS devices image is scanned, and the continuous curves in the image are numbered and stored.

(2) The unprocessed and stored curves in the image are tested in turn. If they cannot be found, the algorithm ends.

(3) The least squares algorithm is used for the pixels on the curve.

(4) The variance of the pixel distribution of the curve is obtained by the least square algorithm. If the variance of the distribution is less than the set value, the curve is a pseudo crack, and the pixel points of the curve should be removed. Otherwise, the pixel points of the curve are retained.

The pseudo-cracks are removed from Figure 6 after Canny operator extracts the edge features of the defect image, and the MEMS devices image after removing the pseudo-cracks is obtained, as shown in Figure 7.

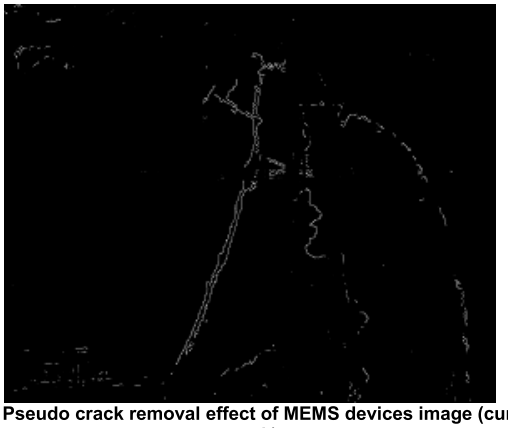

(a) Pseudo crack removal effect of MEMS devices image (curved crack)

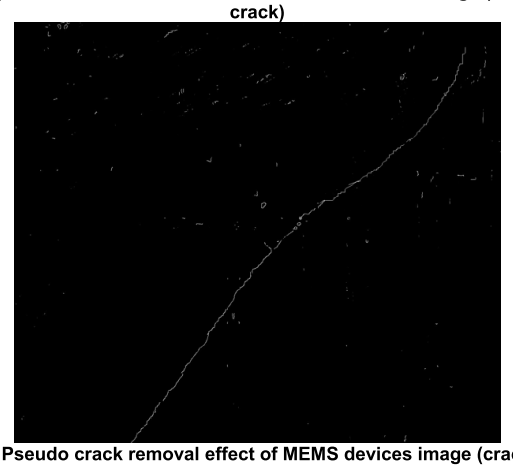

(b) Pseudo crack removal effect of MEMS devices image (cracks penetrating between two metals)

FIGURE 7. Pseudo crack removal effect of MEMS devices image.

Comparing Figures 6 and 7, it can be seen that the pseudo cracks in the images of MEMS devices have been obviously removed, which can effectively improve the accuracy of subsequent crack detection.

III. CRACK DEFECT DETECTION OF MEMS DEVICES IMAGE

When the gray difference between the cracks in the MEMS devices image and the gray level of the device itself is not large, the double peaks in the histogram of the MEMS devices image are not obvious enough, and the effect of the OTSU algorithm is not ideal. In order to improve the detection effect of the algorithm, the attribute weighted naive Bayes algorithm is introduced into the traditional OTSU image processing method [22], [23].

Naive Bayesian classification algorithm is:

$$P(C|X) = \frac{P(X|C)P(C)}{P(X)} \tag{12}$$

where $P(C|X)$ is the posterior probability that condition X belongs to category C; $P(X|C)$ is the posterior probability that category C belongs to condition X; $P(C)$ is the prior probability of class C and $P(X)$ is the prior probability of condition X.

If there are a total of n attribute variables $A(A_1, A_2, \cdots, A_n)$ in the data set, the feature vector $\mathbf{X} = (x_1, x_2, \cdots, x_n)$ represents the specific value of the attribute variable, and there are m category variables C, which have different values $C_1, C_2, \cdots, C_m$, $Test = \langle x_1, x_2, \cdots, x_n \rangle$ as the test set, $Train = \langle x_1, x_2, \cdots, x_n, C_i \rangle$ as the training set. Under the premise of independent assumptions, there is:

$$P(x_1, x_2, L, x_n|C_k) = \prod_{i=1}^{n} p(x_i|C_k), 1 \le k \le m \tag{13}$$

The posterior probability is:

$$P(C_k|x) = \frac{P(C_k)}{P(x)} \prod_{i=1}^{n} p(x_i|c_k), 1 \le k \le m \tag{14}$$

If $P(x)$ is a constant, the naive Bayesian model is:

$$C(x)_N = \arg_i P(C_k) \prod_{i=1}^{n} p(x_i|C_k), 1 \le k \le m \tag{15}$$

In order to improve and enhance the classification effect of the traditional Naive Bayes algorithm, different weights are given to each type of attribute according to the degree of influence of each type of attribute on the classification. This method not only has the high classification accuracy of the traditional naive Bayes algorithm, but also reduces the negative impact of the association between certain attributes in practice. The formula of attribute weighted optimization naive Bayesian model is:

$$C(x)_{N\omega} = \arg_i P(C_k) \prod_{i=1}^{n} p(x_i|C_k)^{\omega(i)}, 1 \le k \le m \tag{16}$$

where $\omega(i)$ is the weight value of class attributeA_i.

In MEMS devices image processing, the MEMS devices image is converted into a grayscale image. The grayscale image is a two-dimensional matrix, so the pixels in the MEMS devices image are discrete data. The segmentation of the OTSU algorithm can also be regarded as a grayscale classification [24], [25]. Based on this feature, the attribute weighted naive Bayesian algorithm is used to improve the OTSU algorithm.

Assuming that the total number of pixels is N gray imageG_N; the gray level is L_N and the gray histogram is

$H_N = \{h_{N0}, h_{N1}, \cdots, h_{NL-1}\}$. Therefore, the gray probability density of e is $p(e) = n(e)/N, e = 0, 1, \cdots L-1$, and $n(e)$ represents the number of pixels when the gray level is e, then: $\sum_{e=0}^{L-1} p(e) = 1$. Let the initial threshold value $T = 1$, the original crack gray image is divided into two parts: G_{N0} and G_{N1}, then the gray level probability of G_{N0} is:

$$p(G_{N0}) = \sum_{e=0}^{T} p(e) \tag{17}$$

The average probability of each gray level in G_{N0} is:

$$\overline{M}(G_{N0}) = \frac{\sum_{e=1}^{T} e \cdot \omega_{e0} \cdot p(G_{N0}|e) \cdot p(e)}{p(G_{N0})} \tag{18}$$

where ω_{e0} is the weighting coefficient, $\omega_{e0} = \frac{GR(e)}{\sum_{e=0}^{T} GR(e)}$, $GR(e)$ is the gain rate of the gray level e.

The average probability of each gray level in G_{N0} becomes:

$$\overline{M}(G_{N0}) = \frac{\sum_{e=1}^{T} e \cdot \omega_{e} \cdot p(G_{N0}|e)}{p(G_{N0})} \tag{19}$$

Similarly, the average probability of each gray level in G_{N1} is:

$$\overline{M}(G_{N1}) = \frac{\sum_{e=T+1}^{L-1} e \cdot \omega_{e1} \cdot p(G_{N1}|e)}{p(G_{N1})} \tag{20}$$

where ω_{e1} is the weight coefficient of each gray level in G_{N1}, $\omega_{e1} = \frac{GR(e)}{\sum_{e=T+1}^{L-1} GR(e)}$.

Therefore, the mean value of the original grayscale image is:

$$\overline{M}_G = \sum_{e=0}^{L-1} e \cdot p(e) \tag{21}$$

Because the image is divided into two categories to calculate the maximum variance between the two parts, the variance of the G_{N0} part is:

$$\begin{aligned}\delta_{N0}^2 = {} & p(G_{N0}) \cdot (\overline{M}(G_{N0}) - \overline{M}_G)^2 \\ & + p(G_{N1}) \cdot (\overline{M}(G_{N1}) - \overline{M}_{NG})^2\end{aligned} \tag{22}$$

The overall variance of the original grayscale image is:

$$\delta_G^2 = \sum_{e=0}^{L-1} (e - \overline{M}_G)^2 \cdot p(e) \tag{23}$$

The crack detection results are shown in Figure 8.

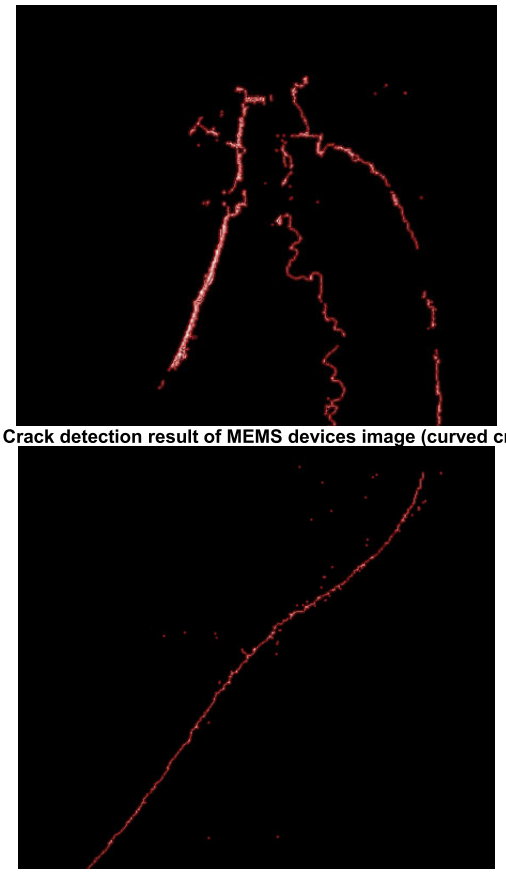

(a) Crack detection result of MEMS devices image (curved cracks)

(b) Crack detection result of MEMS devices image (cracks penetrating between two metals)

FIGURE 8. Crack detection result of MEMS devices image.

IV. QUANTITATIVE CHARACTERIZATION OF CRACK DEFECTS of MEMS DEVICES IMAGE

The crack defects are segmented by MEMS devices image processing. In order to improve the accuracy of crack measurement, the crack is quantitatively characterized on the basis of the segmented crack image, and the length and width of the crack are calculated. It is necessary to extract the crack skeleton first, and the Zhang-Suen refinement algorithm is used to extract the crack skeleton of the MEMS devices image [26].

A. CRACK DEFECT LENGTH

The steps of crack length calculation are as follows:

(1) The crack skeleton diagram is divided into n regions, and the distance between each point in each region is calculated.

(2) Take the longest distance as the crack length in the region:

$$l_k = \max\left\{\sqrt{(x_j - x_k)^2 + (y_j - y_k)^2}\right\} \tag{24}$$

where $j = 1, 2, \cdots, n, k = 1, 2, \cdots, n$, and $j \neq k$.

(3) Add the crack lengths of n rectangular regions, and the total length of the crack is:

$$l = \sum_{k=1}^{n} l_k \tag{25}$$

B. CRACK DEFECT WIDTH

The flow chart of crack width calculation is shown in Figure 9.

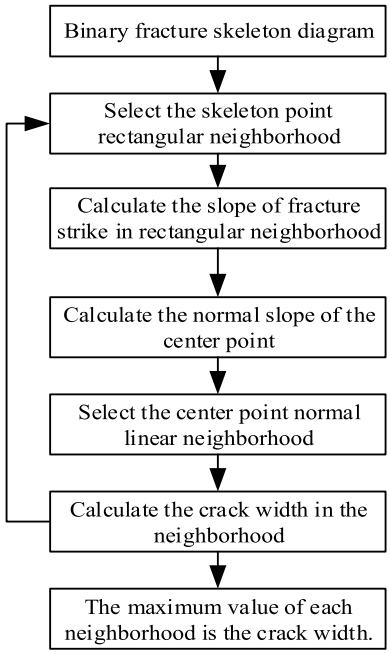

FIGURE 9. Flow chart of crack width calculation.

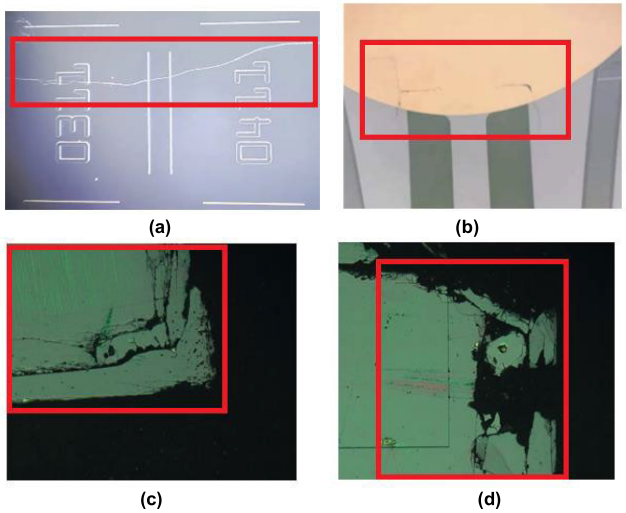

FIGURE 10. The collected original image. (a) Original image 1; (b) Original image 2; (c) Original image 3; (d) Original image 4.

Select a point of the crack on the MEMS devices image, and select a rectangular neighborhood region of the point,

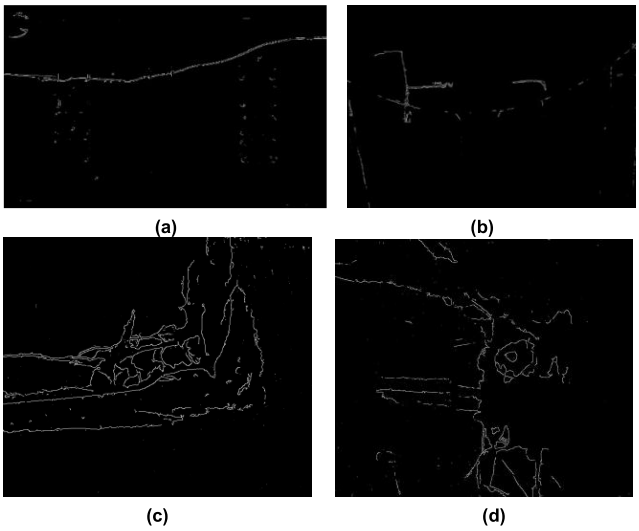

FIGURE 11. The original image after processing. (a) Original image 1 after processing; (b) Original image 2 after processing; (c) Original image 3 after processing; (d) Original image 4 after processing.

then calculate the width of the crack in each rectangular neighborhood. Let D be the radius of the neighborhood and A be the linear neighborhood, then:

$$A = (I_g(x_0, y_0), I_g(x_1, y_1), \cdots, I_g(x_{2D}, y_{2D})) \tag{26}$$

where $I_g(x_D, y_D)$ is the crack point and (x_i, y_i) is the neighborhood point coordinate.

The mean and standard deviation of the MEMS devices image in the neighborhood are defined as:

$$\begin{cases} \mu = \sum_{r=a}^{b} R_m P(R_m) \\ \sigma = \sqrt{\sum_{m=a}^{b} (R_m - \mu)^2 P(R_m)} \end{cases} \tag{27}$$

The variable P_{o1} is set to represent the boundary of one side of the crack, which is:

$$\begin{cases} P_{o1} = I_g(x_{D-o1}, y_{D-o1}), \\ P_{o1} \le \mu - \sigma, \ P_{o1+1} > \mu - \sigma, \\ o1 = 0, 1, \cdots, D. \end{cases} \tag{28}$$

Similarly, the scalar P_{o2} is defined to calculate the other side boundary, which is:

$$\begin{cases} P_{o2} = I_g(x_{D-o2}, y_{D-o2}), \\ P_{o2} \le \mu - \sigma, \ P_{o2+1} > \mu - \sigma, \\ o2 = 0, 1, \cdots, D. \end{cases} \tag{29}$$

The width of the crack is calculated as:

$$width = o1 + o2 \tag{30}$$

Based on the two images of MEMS devices provided in Figure 1, the quantitative characterization of cracks is obtained by image processing, as shown in Table 1. The

TABLE 1. Quantitative characterization of cracks.

MEMS devices images	Length /μm			Width /μm		
	Manual measurement method	The detection method proposed in this paper	Deviation value	Manual measurement method	The detection method proposed in this paper	Deviation value
Figure 1 (a)	62	67	5	21	26	5
Figure 1 (b)	131	137	6	9	11	2

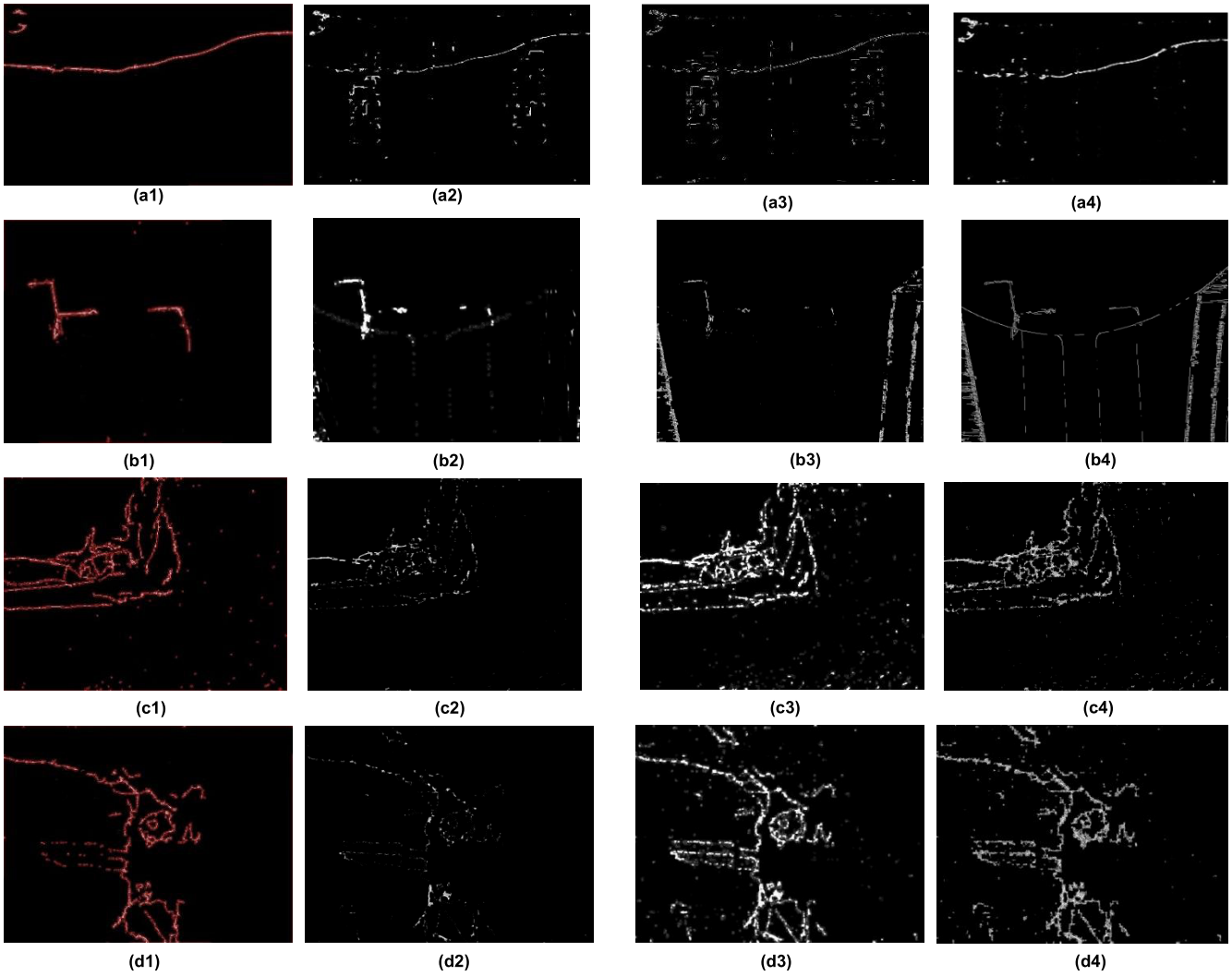

FIGURE 12. Crack detection result of MEMS devices Images.

test results are as follows: the maximum deviation between the proposed method and the actual crack length is 6μm, and the maximum deviation from the actual crack width is 5μm.

V. EXPERIMENTS AND RESULT ANALYSIS

Based on the collected many MEMS devices images with different crack defects, the MEMS devices defect detection method based on image processing proposed in this paper is used for image processing. In order to verify the detection accuracy of this method, a comparative test of detection accuracy is carried out. The original images of different MEMS devices are shown in Figure 10. In Figure 10, there are some crack defects in the red frame. The image obtained by the image processing method proposed in this paper is shown in Figure 11. The crack detection results of the proposed method and other methods in [14], [15], and [27] are shown in Figure 12.

TABLE 2. Crack length test results.

No.	Manual measurement method	The detection method proposed in this paper	Reference [14]	Reference [15]	Reference [27]
Original image 1	215	223	201	204	225
Original image 2	37	33	24	26	43
Original image 3	82	87	71	92	90
Original image 4	64	69	52	72	71

TABLE 3. Crack width test results.

No.	Manual measurement method	The detection method proposed in this paper	Reference [14]	Reference [15]	Reference [27]
Original image 1	17	14	11	9	13
Original image 2	26	28	31	19	29
Original image 3	21	25	10	28	26
Original image 4	19	22	12	25	23

In Figure 12, (a1) - (a4) are the crack detection results of the original image 1 using the method proposed in this paper, the References [14], [15], and [27]; (b1) - (b4) are the crack detection results of the original image 2 using the method proposed in this paper, the References [14], [15], and [27]; (c1) - (c4) are the crack detection results of the original image 3 using the method proposed in this paper, the References [14], [15], and [27]; (d1) - (d4) are the crack detection results of the original image 4 using the method proposed in this paper, the References [14], [15], and [27]. In order to reflect the effect of the proposed method for extracting cracks, the cracks in Figures 12(a1), (b1), (c1) and (d1) were marked, the red part marked the cracks of the MEMS devices, so that the morphology of the cracks, such as length, width and properties, could be seen more directly and clearly.

The collected MEMS devices images are processed, and the OTSU algorithm improved by the naive Bayesian algorithm based on attribute weighting is used to segment the crack information and background information. On the basis of crack skeleton extraction, the length and width of the crack are measured, and the length and width of the crack in the MEMS devices images processed by the methods of References [14], [15], and [27] are measured. The measurement results are shown in Tables 2 and 3.

In Tables 2 and 3, the units of the result are μm. Through Tables 2 and 3, the error between the crack detection results of the method proposed in this paper and the methods of References [14], [15], and [27] and the manual measurement results is obtained. Figure 13 is the crack length error result, and Figure 14 is the crack width error result.

In Figures 13 and 14, e_{l1} and e_{w1} are the absolute error of crack length and crack width obtained by the proposed method and manual measurement method, respectively; e_{l2} and e_{w2} are the absolute error of crack length and crack width obtained by method of Reference [14] and manual measurement method, respectively;e_{l3} and e_{w3} are the absolute error of crack length and crack width obtained by method of Reference [15] and manual measurement method, respectively; e_{l4} and e_{w4} are the absolute error of crack length and crack width obtained by method of Reference [27] and manual measurement method, respectively; n is the number of MEMS devices image. It can be seen from figures 13 and 14 that the maximum absolute errors between the length and width of the crack detected by the proposed method and the manual measurement method are the smallest, which are 8μm and 4μm respectively. The deviation between the detection results of the method proposed in Reference [14] and the manual measurement method is the largest, which is related to its inability to effectively deal with the characteristics of false defects. The deviation between the detection results

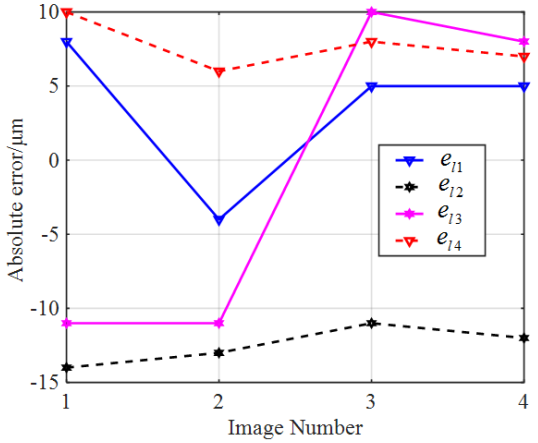

FIGURE 13. Calculation error of crack length.

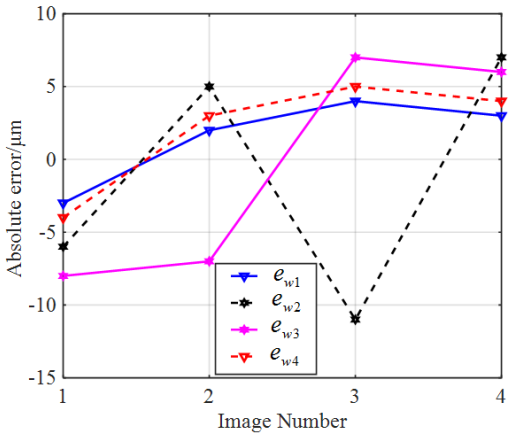

FIGURE 14. Calculation error of crack width.

of the method proposed in Reference [27] and the manual measurement method is close to the deviation between the detection results and the manual measurement method in this paper, which is slightly larger. This is related to the effective training of YOLOv4 network, which can improve the detection accuracy.

In order to verify the superiority of the crack detection method proposed in this paper, the running time of the image processing of the MEMS devices taken by 1000 frames is tested. The methods of this paper, References [14], [15], and [27] are used respectively. The comparison results are shown in Table 4.

TABLE 4. Crack detection comparison results.

Crack test method	Testing time / s	Accuracy of detection
Reference [14]	129.6	47.8%
Reference [15]	311.7	71.3%
Reference [27]	452.0	86.2%
Method of this paper	248.1	94.6%

It can be seen from Table 4 that reference [14] has a great advantage in training time, but the effect of defect detection is not ideal, and the accuracy rate is only 47.8 %. This is mainly through the combination of Kirsch operator and Canny operator to realize the edge detection of surface defects. It is difficult to effectively deal with the problems of uneven illumination or serious noise interference in crack defect images. Compared with the method in Reference [14], the detection method in Reference [15] can effectively improve the accuracy of detection, but its detection time is also greatly increased. The surface defect detection method of electronic components based on improved YOLOv4 is proposed in Reference [27]. Although the accuracy of detecting cracks on MEMS devices is improved compared with References [14] and [15], its detection time is longer, which is not conducive to practical engineering applications. The method proposed in this paper not only has an accuracy of 94.6 %, but also has a relatively short detection time, which is more conducive to the accurate detection of cracks of MEMS devices image in practical engineering experiments.

VI. CONCLUSION

In order to extract the crack information in the MEMS devices image efficiently and accurately, the MEMS devices image is blurred and contains a lot of irrelevant information. The edge of the defect in the MEMS devices image is extracted by image detail sharpening, grayscale processing, image enhancement and edge processing based on Canny operator, and the pseudo crack information similar to the crack defect is removed by the least square method. The crack detection method based on attribute weighted naive Bayes improved OTSU algorithm is studied. The Zhang-Suen refinement algorithm is used to extract the crack skeleton, and the calculation method of crack length and width is established.

Through experimental verification, the method proposed in this paper can accurately detect the cracks of MEMS devices image. The research results provide a detection method for the reliable and stable operation of MEMS devices under high impact. MEMS is a microsystem based on the movable micromechanical chip produced by the combination of microelectronics chip manufacturing technology and precision machinery. It is a new chip technology with distinctive interdisciplinary characteristics, which brings transformative development for the miniaturization, integration and intelligence of mechanical and electrical products. Among, MEMS devices have the advantages of high integration, strong function, light weight, low power consumption, low thermal constant, vibration resistance, shock resistance and radiation resistance; it plays an important role in miniaturization, low cost and performance improvement of the system.

In the fields of consumer electronics and automotive electronics, mass manufacturing technology is vigorously developed through high-volume MEMS devices, while high-end MEMS devices in aerospace and other fields need to develop their customized manufacturing technology in order to obtain MEMS devices that meet special needs. The development trend of MEMS devices in aerospace systems is to replace large and bulky devices on space carriers, communication and navigation platforms and payloads, and finally realize the miniaturization, intelligence and integration of aerospace systems. In the application of MEMS devices in aerospace systems, the radiation, vacuum, thermal shock, vibration and packaging in the space specific working environment directly affect its reliability, so it is necessary to further promote more in-depth research on MEMS devices, especially in the aspect of high reliability. It can be seen that the research work in this paper has certain application value.

REFERENCES

[1] K. Hari, S. K. Verma, I. R. P. Krishna, and V. Seena, "Out-of-plane dual flexure MEMS piezoresistive accelerometer with low cross axis sensitivity," *Microsyst. Technol.*, vol. 24, no. 5, pp. 2437–2444, May 2018.

[2] J. Zhu, X. Liu, Q. Shi, T. He, Z. Sun, X. Guo, W. Liu, O. B. Sulaiman, B. Dong, and C. Lee, "Development trends and perspectives of future sensors and MEMS/NEMS," *Micromachines*, vol. 11, no. 7, pp. 1–30, Jan. 2020.
[3] Y. Wang, J. Zhao, and P. Liu, "Design and experimental error analysis of triaxial accelerometer based on PZT tube support structure," *Chin. J. Sci. Instrum.*, vol. 41, no. 7, pp. 91–98, 2020.
[4] K. Li, T. Jiang, X. Guo, S. Li, L. Zhang, X. Zhang, and S. Mou, "Design of three-mass MEMS triaxial capacitive accelerometer," *J. Electron. Meas. Instrum.*, vol. 35, no. 10, pp. 193–201, 2021.
[5] Y. Yang, P. Wang, M. Chen, C. Zhang, F. Yang, and F. Chen, "Simulation design of high G value piezoresistive acceleration sensor," *Transducer Microsyst. Technol.*, vol. 41, no. 6, pp. 78–82, 2022.
[6] J. He, W. Gao, H. Wang, B. Yue, F. Zhang, and Z. Zhang, "Wheel steering angle measurement method of agricultural machinery based on GNSS heading differential and MEMS gyroscope," *J. South China Agricult. Univ.*, vol. 41, no. 5, pp. 91–98, 2020.
[7] W. Tian, X. Wang, and J. Luo, "Spacecraft hidden target point measurement based on MEMS laser radar," *Comput. Meas. Control*, vol. 28, no. 3, pp. 1–5, 2020.
[8] C. Zhang, Y. He, J. Xie, and D. Wang, "Optimization of overload power of capacitive MEMS microwave power sensor," *Microelectronics*, vol. 51, no. 3, pp. 434–438, 2021.
[9] A. A. Umanskii, A. S. Simachev, A. V. Golovatenko, and L. V. Dumova, "Nature detection of internal defects in railroad rails produced by EVRAZ ZSMK company using ultrasonic control in mill flow," *Metal Sci. Heat Treatment*, vol. 64, nos. 5–6, pp. 350–354, Sep. 2022.
[10] H. Liu, X. Jia, C. Su, H. Yang, and C. Li, "Tire appearance defect detection method via combining HOG and LBP features," *Frontiers Phys.*, vol. 10, Jan. 2023, Art. no. 1099261.
[11] Y. Shang, C. Liu, J. Wang, X. Kong, Y. He, and H. Wei, "Machine vision inspection of surface defects of stamping blank," *Modular Mach. Tool Autom. Manuf. Technique*, vol. 12, pp. 85–88, Apr. 2022.
[12] Z. He, Y. Wang, J. Liu, and F. Yin, "Background differencing-based high-speed rail surface defect image segmentation," *IEEE Trans. Circuits Syst. Video Technol.*, vol. 37, no. 3, pp. 640–649, May 2016.
[13] M. Guo, L. Hu, and J. Zhao, "Surface defect detection method of ceramic bowl based on Kirsch and Canny operator," *Acta Optica Sinica*, vol. 36, no. 9, pp. 27–33, 2016.
[14] X. Liu, L. Zhu, Y. Wang, and Z. Yu, "A crack detection system of subway tunnel based on image processing," *Meas. Control*, vol. 55, nos. 3–4, pp. 164–177, Mar. 2022.
[15] H. Jung, C. Lee, and G. Park, "Fast and non-invasive surface crack detection of press panels using image processing," *Proc. Eng.*, vol. 188, pp. 72–79, Jan. 2017.
[16] H. Lv, H. Xia, J. Luo, and L. Liu, "Surface defect detection of electronic components based on machine vision," *Electron. Product Rel. Environ.*, vol. 39, no. 1, pp. 18–21, 2021.
[17] X. G. Li, Q. W. Huang, Y. H. Wang, Y. B. Jia, and Z. B. Wang, "The response of electrostatic MEMS structure under mechanical shock and electrostatic forces," *Appl. Mech. Mater.*, vols. 427–429, pp. 120–123, Sep. 2013.
[18] D. Wang and T. Shen, "Research on weak and small infrared target detection algorithm under complex sky background," *Acta Optica Sinica*, vol. 40, no. 5, pp. 103–110, 2020.
[19] M. Liu, X. Xue, G. Liu, Z. Liu, and H. Cai, "Contrast enhancement algorithm for gray scale of color images," *J. Changchun Univ. Sci. Technol.*, vol. 41, no. 5, pp. 70–74, 2018.
[20] Y. Mousania, S. Karimi, and A. Farmani, "Optical remote sensing, brightness preserving and contrast enhancement of medical images using histogram equalization with minimum cross-entropy-Otsu algorithm," *Opt. Quantum Electron.*, vol. 55, no. 2, p. 105, Feb. 2023.
[21] A. Lapusinskij, I. Suzdalev, N. Goranin, J. Janulevicius, S. Ramanauskaite, and G. Stankunavicius, "The application of Hough transform and Canny edge detector methods for the visual detection of cumuliform clouds," *Sensors*, vol. 21, no. 17, p. 5821, Aug. 2021.
[22] Y. Wang, Y. Huang, K. Yang, Z. Chen, and C. Luo, "Generator fault classification method based on multi-source information fusion naive Bayes classification algorithm," *Energies*, vol. 15, no. 24, p. 9635, Dec. 2022.
[23] W. Zhang, Z. Wang, J. Yuan, and H. Liu, "A locally attribute weighted naive Bayes classifier," *J. Beijing Jiaotong Univ.*, vol. 42, no. 2, pp. 14–21, 2018.
[24] Y. Bao, L. Zhou, and P. Duan, "A weighted naive Bayes classification algorithm based on a genetic algorithm," *J. Yunnan Minzu Univ.*, vol. 27, no. 6, pp. 525–529, 2018.
[25] S. Shi, P. Feng, and Q. Sun, "An algorithm for target extraction based on Bayesian estimation and multi between-cluster variance," *J. Projectiles, Rockets, Missiles Guid.*, vol. 40, no. 2, pp. 32–34, 2020.
[26] Y. Wu, J. Wang, and Y. Wang, "'Crop stem recognition and localization method based on skeleton extraction algorithm," *Trans. Chin. Soc. Agricult. Machinery*, vol. 53, no. 11, pp. 334–340, 2022.
[27] F. Wen and Y. Chen, "Research on surface defect detection technology of electronic components based on improved YOLOv4," *J. Shenyang Ligong Univ.*, vol. 40, no. 2, pp. 1–8, 2021.

YU ZHENG received the bachelor's degree in applied physics from Jilin University, in 2008. He is currently a Senior Engineer with the East China Institute of Photo-Electron IC, mainly engaged in the research and development of MEMS devices and integrated circuits and research on testing technology.

SUSU LI received the bachelor's degree in environmental engineering from the Anhui University of Science and Technology, in 2005. She is currently a Senior Engineer with the East China Institute of Photo-Electron IC, mainly engaged in the research and development of MEMS devices and integrated circuits.

YUAN XIANG received the B.S. degree in material forming and control engineering from the Huazhong University of Science and Technology, in 2011. He is currently a Senior Engineer with the East China Institute of Photo-Electron IC, mainly engaged in research on packaging technology of special devices and integrated product groups.

ZHENXING ZHU received the B.S. degree in communication engineering from the Nanjing University of Science and Technology, Nanjing, China, in 2010, and the M.S. degree in communication and information system from Xi'an Technological University, Xi'an, China, in 2013. He is currently a Senior Engineer with the East China Institute of Photo-Electron IC, where he is engaged in research and development of semiconductor integrated circuit and hybrid integrated circuit.